J. Fluid Mech. (2003), *vol.* 492, *pp.* 271–287.
DOI: 10.1017/S0022112003005640 Printed in the United Kingdom

Experiments on highly supercritical thermal convection in a rapidly rotating hemispherical shell

By IKURO SUMITA[1] AND PETER OLSON[2]

[1]Department of Earth Sciences, Kanazawa University, Kanazawa, Ishikawa, 920-1192, Japan

[2]Department of Earth and Planetary Sciences, Johns Hopkins University, Baltimore, MD 21218, USA

(Received 27 June 2002 and in revised form 13 December 2002)

We report experimental results on highly supercritical thermal convection in a rapidly rotating hemispherical shell with parabolic gravity. Using silicone oil as the working fluid and an Ekman number $Ek = 4.7 \times 10^{-6}$ we reach Rayleigh numbers up to 1.2×10^{10}, over 600 times critical. *In-situ* temperature measurements show that, at these highly supercritical states where convective heat transfer becomes dominant, the time-averaged temperature in the fluid becomes nearly uniform except in a thin thermal boundary layer near the inner spherical boundary. Heat transfer measurements show that Nusselt number Nu increases with Rayleigh number Ra as $Nu \propto Ra^{0.4}$. The measured amplitudes of temperature fluctuations scale well with a model of geostrophic convective turbulence. We also examine convection in a two-layer fluid in the same geometry, using layers of water and silicone oil to produce a stable density stratification. We determine the dependence of heat transfer on the thickness ratio of the layers.

1. Introduction

Thermal convection in a rapidly rotating spherical shell is the basic model for convection in planetary cores and stellar interiors. A large number of theoretical, numerical, and experimental studies have been made in order to understand this style of convection (for a recent review, see Zhang & Schubert 2000). The linear regime (near the onset of convection) has been investigated analytically (e.g. Jones, Soward & Mussa 2000 and references therein), and the basic structures in the weakly nonlinear regime have been investigated numerically (e.g. Zhang 1992). Laboratory experiments have also played an important role, where the centrifugal force is substituted for radially dependent gravity, a technique first used by Busse & Carrigan (1974, 1976). At low Ekman (Ek) and high Rayleigh (Ra) numbers (see table 1 for the definitions of these and other parameters), which is the relevant regime for planetary cores, convection is characterized by fine-scaled, quasi-geostrophic turbulence. Quasi-geostrophic convective turbulence is easily attained in laboratory experiments using rapidly rotating spheres and hemispheres. High-Rayleigh-number ($Ra/Ra_c > 10$) thermal convection at low Ekman number ($Ek = 10^{-6}$) was studied by Cardin & Olson (1994), using water (Prandtl number $Pr = 7.1$) as the working fluid, and they proposed a scaling law applicable to high-Rayleigh-number conditions. Sumita & Olson (2000) used the hemispherical shell geometry to examine the flow pattern and thermal structure at $Ek = 4.7 \times 10^{-6}$ and $Ra/Ra_c < 45$, also using water

Property	Units	Water	1 cSt silcone oil
Density ρ	kg m^{-3}	1000	816
Heat capacity C_p	J kg^{-1} K^{-1}	4182.0	1716.1
Kinematic viscosity ν	m^2 s^{-1}	1.0×10^{-6}	1.0×10^{-6}
Thermal conductivity k_T	W m^{-1} K^{-1}	0.594	0.100
Thermal diffusivity κ	m^2 s^{-1}	1.42×10^{-7}	7.17×10^{-8}
Thermal expansivity α	K^{-1}	2.1×10^{-4}	1.34×10^{-3}
Prandtl number Pr	none	7.1	13.9
Ekman number Ek	none	4.66×10^{-6}	4.64×10^{-6}
Rayleigh number Ra	none	1.8×10^8–9.4×10^{8} [a]	1.24×10^9–1.24×10^{10}
Ra/Ra_c [b]	none	10–52	63–634

TABLE 1. Dimensionless numbers and parameters and their values in the experiments. Properties of water are at 20 °C, silicone oil are at 25 °C. $Pr = \nu/\kappa$, $Ek = \nu/(\Omega D^2)$, $Ra = \alpha g \Delta T D^3/(\kappa \nu)$, $Nu = Q_{IC}/(k \Delta T/D)$, Q_{IC}: inner sphere heat flow (W), $g = \Omega D^2$: centrifugal acceleration, Ω: angular velocity of rotation, D: shell thickness, ΔT: temperature difference across the shell. [a] For the data points used in figure 2. [b] See text for critical Rayleigh number (Ra_c) values.

as the working fluid. Aubert *et al.* (2001) made detailed velocity measurements in a spherical shell with a cylindrical inner core, using water at $Ek = 10^{-5}$ to 10^{-6} and $3 < Ra/Ra_c < 80$, as well as liquid gallium ($Pr \simeq 0.025$) at $Ek = 10^{-6}$ to 10^{-7} and $1 < Ra/Ra_c < 10$.

In this paper, we extend the experiments of Sumita & Olson (2000), using silicone oil as the working fluid. This allows us to reach Rayleigh numbers up to 1.2×10^{10} ($\sim 634 Ra_c$), an order of magnitude higher than that in Sumita & Olson (2000) yet at the same Ekman number and a similar Prandtl number. The range of Rayleigh numbers in our experiments include the highest case studied by Boubnov & Golitsyn (1986, 1990), in a regime they have called "irregular geostrophic turbulence".

By combining our experiments with lower-Rayleigh-number experiments by Sumita & Olson (2000), we derive power-law relationships for heat transfer and temperature fluctuations over 3 orders of magnitude in the Rayleigh number. We find that these relationships closely match predictions for these variables derived for the asymptotic regime of rapidly rotating spherical shell convection.

2. Experimental method

The experimental apparatus shown in figure 1 is essentially the same as that used in Sumita & Olson (2000). It consists of a hemispherical shell of thickness 10 cm, with the temperature of the inner sphere fixed at a lower temperature than the working fluid by cooling fluid circulated through the inner sphere. The hemisphere is rotated steadily at 206 r.p.m., the same rate as in Sumita & Olson (2000). The combined effect of the centrifugal force and laboratory gravity produces parabolic equipotential surfaces. The equatorial lid is relatively unimportant beyond the critical Rayleigh number, as evidenced by the fact that we observe essentially the same flow patterns as seen in experiments using full spherical shells (Cardin & Olson 1994; Manneville & Olson 1996; Aubert *et al.* 2001).

Temperature is measured using thermistor probes. Hypodermic-type probes (YSI model 552) are used for measuring the fluid temperature at a depth (<1 mm) beneath the equatorial plane. A catheter-type probe (YSI model 555) is used for measuring

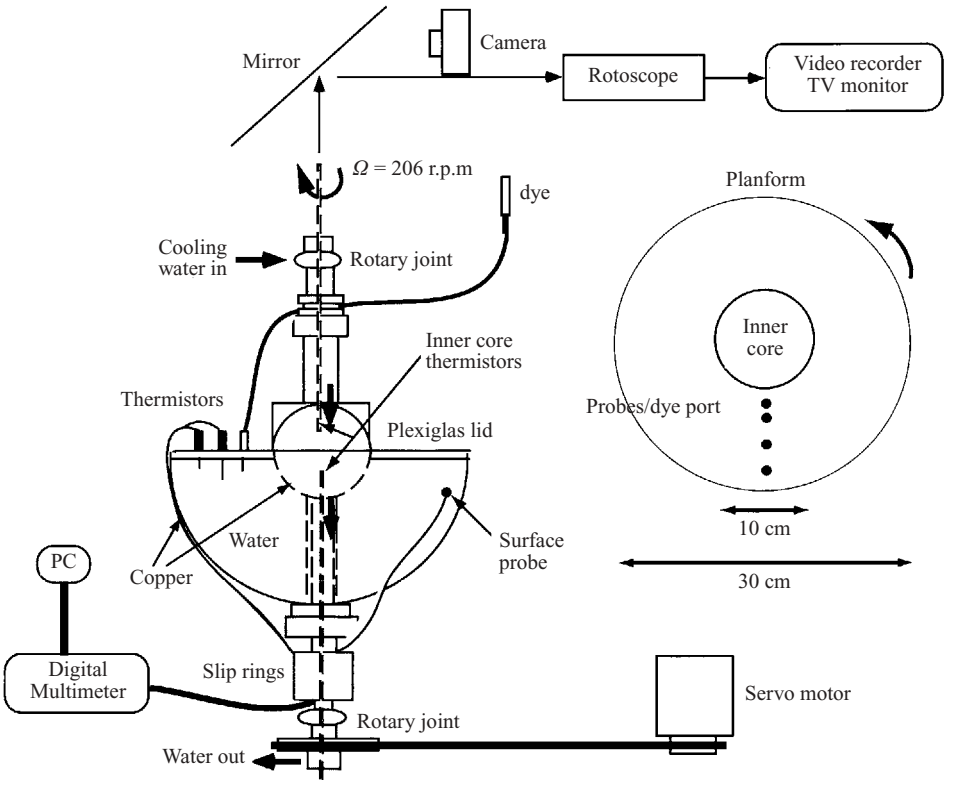

FIGURE 1. A sketch of the experimental apparatus.

the temperature of the cooling fluid entering (T_{in}) and exiting (T_{out}) the inner sphere. We use T_{out} as the inner-sphere boundary temperature, and we use $\Delta T_{IC} = T_{out} - T_{in}$ to calculate the heat flow at the inner boundary. Surface-type thermistor probes (YSI model 409B) are attached to the outer boundary. These probes were calibrated to an accuracy of 0.01 °C. The sampling frequency of the probes is $\leqslant 1$ Hz, which is commensurate with the 0.2 s time constant of the hypodermic probe.

We use water and 1 cSt Dow Corning 200 silicone oil, whose properties are summarized in table 1. These fluids have virtually the same kinematic viscosity, which allows us to achieve comparable Ekman numbers using the same rotation rate. As can be seen in table 1, because of the differences in thermal diffusivity and thermal expansivity, the ranges of the Rayleigh number achieved by water and silicone oil are complementary. The temperature dependence of kinematic viscosity is small for both fluids, and is less than a factor of about 1.8 for water and about 1.3 for silicone oil for the largest experimental temperature range of 0–20 °C.

The critical Rayleigh number for the onset of convection in water ($Pr = 7.1$) at $Ek = 4.7 \times 10^{-6}$ was estimated experimentally by Sumita & Olson (2000) as $Ra_c = 1.8 \times 10^7$, close to $Ra_c = 2.3 \times 10^7$ at $Ek = 4.8 \times 10^{-6}$ obtained numerically by Aubert *et al.* (2001). In this study we adopt our experimental value of $Ra_c = 1.8 \times 10^7$ for water. We could not determine Ra_c for silicone oil from our experiments because of the difficulty in maintaining very small temperature differences across the shell, of the order of 10^{-2} °C. Instead we convert our critical Rayleigh number for water to the critical Rayleigh number for silicone oil ($Pr = 13.9$), using the analytical model

of Busse (1970). This procedure gives $Ra_c = 1.96 \times 10^7$ for silicone oil. According to the analysis of Jones *et al.* (2000) and Zhang & Schubert (2000), the wavenumber of the instability at the onset of convection in water and silicone oil is expected to be approximately the same.

The experimental procedure is as follows. The hemisphere is spun up from rest to a steady rotation rate, and then the temperature difference across the hemisphere is imposed. For the silicone oil experiments shown in figure 2, the lowest imposed temperature at the inner core boundary T_{out} is 2.2 °C, and the highest T_{out} is 23.0 °C. These correspond to the highest and lowest Rayleigh number cases, respectively. We monitor the temperature at the boundaries and the heat flow at the inner boundary until thermal equilibrium is achieved, which typically takes 2–3 hours. After equilibrium is reached, continuous measurements of temperature in the fluid are made for about 30 minutes. In some experiments, we then made flow velocity measurements in the silicone oil by releasing neutrally buoyant tracer material, a solution of methyl alcohol and a fluorescent dye. In the two-layered convection experiments, the hemisphere was filled with various volumetric ratios of water and silicone oil, and the procedures used in the single-layer experiments were repeated. In addition, the convective pattern in the outer layer was visualized using Kalliroscope flakes.

3. Results

3.1. *Single-layer experiments*

3.1.1. *Time-averaged thermal structure*

Figure 2 shows how the radial temperature profile changes with Rayleigh number. The figure compares results from our silicone oil experiments with experiments in water from Sumita & Olson (2000, 2002). The temperature profiles in figure 2 are normalized by the temperature difference across the shell, so that 0 corresponds to the temperature at the inner boundary and 1 to the temperature at the outer boundary. Temperatures at four different radial distances (1.5, 3.1, 5.6, and 8.1 cm) from the inner boundary are shown. As the Rayleigh number increases, the normalized temperatures in the fluid asymptotically approach the temperature of the outer boundary, while the temperature difference across the thermal boundary layer adjacent to the inner boundary approaches unity, and the thickness of the thermal boundary layer diminishes. All of these trends are expected consequences of increased convective heat transfer. The temperature for the equivalent conductive profile in a spherical shell at radial distances of 3.1, 5.6, and 8.1 cm, respectively, from the inner boundary are indicated by arrows in figure 2. These are close to the temperatures measured at the same locations for convection at $Ra/Ra_c \simeq 10$, an indication that the convective contribution to the total heat transfer is small when the Rayleigh number is only ten times critical. Note that the results from silicone oil and water experiments form a continuous trend in figure 2, confirming that 1 cSt silicone oil can be used as an alternative to water for exploring higher Rayleigh number regimes of convection.

Figure 3 shows standard deviations of temperature fluctuations normalized by the temperature difference across the shell, as a function of Rayleigh number. Note that the normalized fluctuations decrease with increasing Rayleigh number. Combined visualization and temperature measurements in water show that rotating spherical convection is dominated by quasi-geostrophic (columnar) flow driven by cold and warm plumes. These plumes advect heat in the radial direction, especially near the

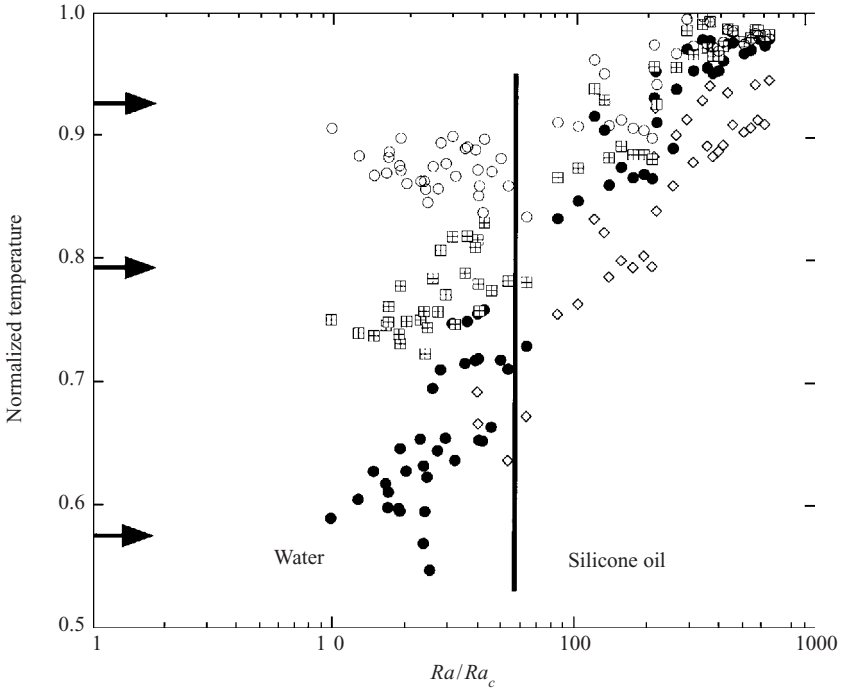

FIGURE 2. Rayleigh number dependence of the temperature for thermal convection in the equatorial plane of a rotating hemispherical shell. Measurements taken at distances of $r = 1.5$, 3.1, 5.6 and 8.1 cm (◇, ●, ⊞, ○), respectively, from the inner boundary. The data for water are in the dual convective regime identified by Sumita & Olson (2000). Temperatures are normalized by the temperature difference across the shell. The arrows indicate the equivalent conduction-state temperature for the probes at $r = 3.1$, 5.6 and 8.1 cm.

equatorial plane, and their amplitudes reflect the background temperature gradient. We can similarly interpret the result shown in figure 3 as a consequence of the smaller temperature gradient in the fluid as the Rayleigh number increases, which is consistent with figure 2.

The time-averaged thermal structure of single-layer hemispherical convection is indicated in figure 4, which shows the relation between the temperature difference across the shell ΔT and the temperature rise of the water circulating through the inner sphere, ΔT_{IC}. Since ΔT_{IC} is proportional to the heat flow at the inner boundary Q_{IC}, we use this to compute the Nusselt number and its Rayleigh number dependence, using the method of Sumita & Olson (2000). Since $Nu \propto \Delta T_{\mathrm{IC}}/\Delta T$ and $Ra \propto \Delta T$, after fitting the data as $\Delta T_{\mathrm{IC}} \propto \Delta T^n$, we obtain $Nu \propto Ra^{n-1}$. Because ΔT_{IC} is more accurate for large ΔT, we use the data corresponding to large ΔT in order to minimize the relative error in n (i.e. $\delta n/n$). The data for $Ra/Ra_c \geqslant 212$ gives $n = 1.41 \pm 0.02$ (with a correlation coefficient of $R = 0.997$). This, in turn, yields $Nu \propto Ra^{0.41}$, which is slightly larger than the classic Rayleigh number–Nusselt number power-law exponent 1/3 predicted from boundary layer stability. We note, however, that accurate determination of the power-law exponent is difficult in our apparatus because of the limited accuracy of the thermistor probes (about $< 0.01\,^{\circ}\mathrm{C}$). Assuming a maximum error of $0.01\,^{\circ}\mathrm{C}$ for ΔT_{IC}, we find that the range of power-law exponents consistent with our data is 0.41 ± 0.10. We also compute the Nusselt number defined as $Nu = Q_{\mathrm{IC}}/(k\Delta T/D)$ using $Q_{\mathrm{IC}} \simeq 16(\Delta T_{\mathrm{IC}}/0.1\,\mathrm{K})\mathrm{W}$ (Sumita &

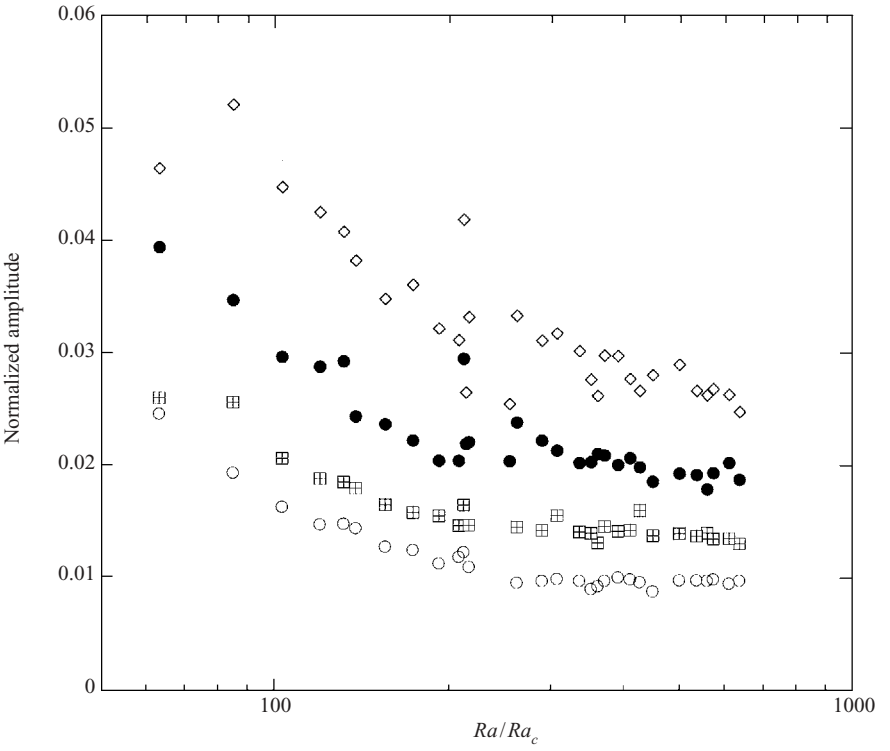

FIGURE 3. Rayleigh number dependence of the standard deviation of temperature fluctuations for four probes at different distances from the inner boundary, near the equatorial plane. Here, the standard deviation is normalized by the temperature difference across the shell.

Olson 2000). We then find that the range of Nu for the experiments using silicone oil ($1.24 \times 10^9 < Ra < 1.24 \times 10^{10}$) is 40–186.

Figure 5 shows the standard deviation of temperature fluctuations versus ΔT_{IC} at four different radial points in the fluid. We use the large-ΔT_{IC} data from each probe to obtain the power-law fit, so that the relative error of the slope b (i.e. σ_b/b) gives a local minimum. The power-law exponents obtained this way for the three inner probes are close to $n = 0.6$, consistent with the model of turbulent columnar convection of Cardin & Olson (1994), Aubert *et al.* (2001) and Sumita & Olson (2002) for water. This agreement indicates that the same scaling law is applicable for the experiments using silicone oil.

3.1.2. *Time-dependent thermal structure*

The time-dependent features of the temperature records can be interpreted in terms of the structure of the flow. Figure 6 shows examples of temperature time series at several Rayleigh numbers, recorded at probes located near the inner and outer boundaries, respectively. In these records, the temperature is normalized by the temperature difference across the shell ΔT. As a result of this particular normalization, high-frequency temperature fluctuations due to background thermal noise tend to be magnified in experiments where ΔT is small (see figure 6*b*). With increasing Rayleigh number the time-average temperature of the innermost and outermost probes approach each other, and the (normalized) amplitude of temperature fluctuations becomes smaller. The temperature fluctuations are generally irregular, although they

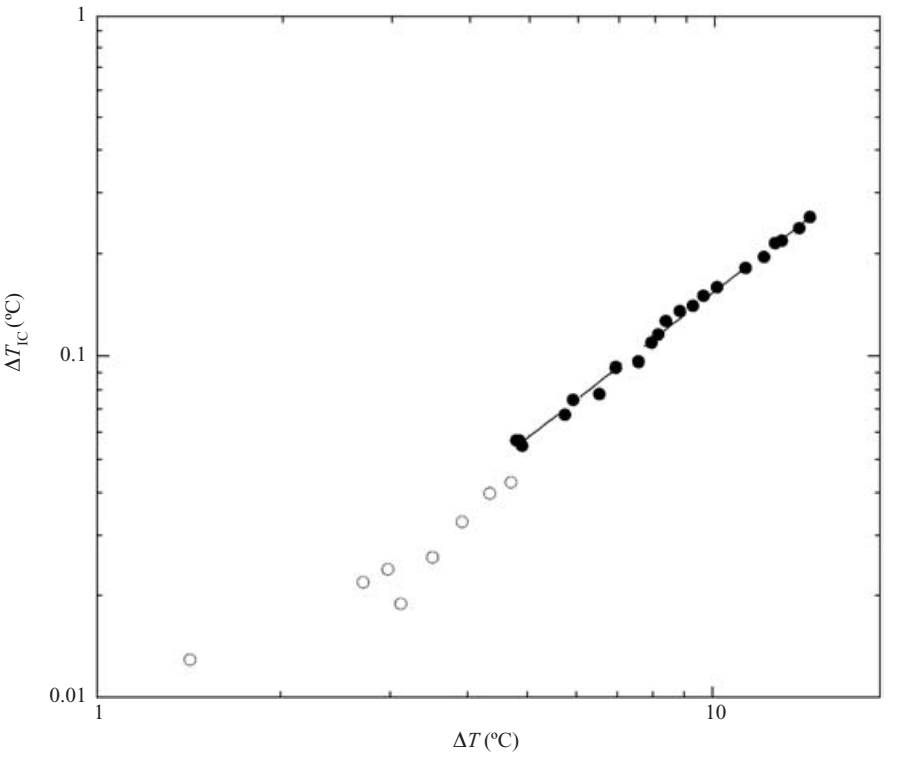

FIGURE 4. Relation between the imposed temperature difference across the shell ΔT, and the temperature rise of the circulating water through the inner sphere ΔT_{IC}. Data points in solid circles are used to obtain a power-law fit of $\Delta T_{IC} = 0.006\Delta T^{1.41\pm0.02}$ (correlation coefficient 0.997).

show occasional, predominant negative, spikes. Also we find that the frequency of temperature fluctuations increase with Rayleigh number.

Figure 7 shows a histogram of the temperatures from the time series records in figure 6. The temperature bins are normalized by the standard deviation of the record. Note that the histogram is asymmetric, with the length of the negative tail about four times the standard deviation. The asymmetry of this histogram can be interpreted quantitatively using the skewness S of the distribution, $S = \langle (T - \langle T \rangle)^3 \rangle / \langle (T - \langle T \rangle)^2 \rangle^{3/2}$ where $\langle\ \rangle$ denotes the average over all data points in the record. We find that the skewness of the temperature records is negative for all probes in all of our experiments. The skewness ranges from $S \simeq -0.5$ near the inner boundary to $S \simeq -0.1$ near the outer boundary. There is no clear dependence of the skewness on the Rayleigh number, which is evident from the similarity of the shape of the histogram for different Rayleigh numbers in figure 7.

We next examine the time derivative of temperature fluctuations S', a statistic which has been used to interpret convective turbulence by Belmonte & Libchaber (1996) and by Sumita & Olson (2002). We find that S' is negative near the inner boundary (about -0.4 for the innermost probe) and tends to zero near the outer boundary. Previous experiments (Sumita & Olson 2002) have shown that this is a result of the saw-tooth pattern of temperature fluctuations. A negative S' indicates a fluctuation with a steep decrease followed by a gradual increase. Two interpretations of the observed negative S' have been suggested. Belmonte & Libchaber (1996) interpreted

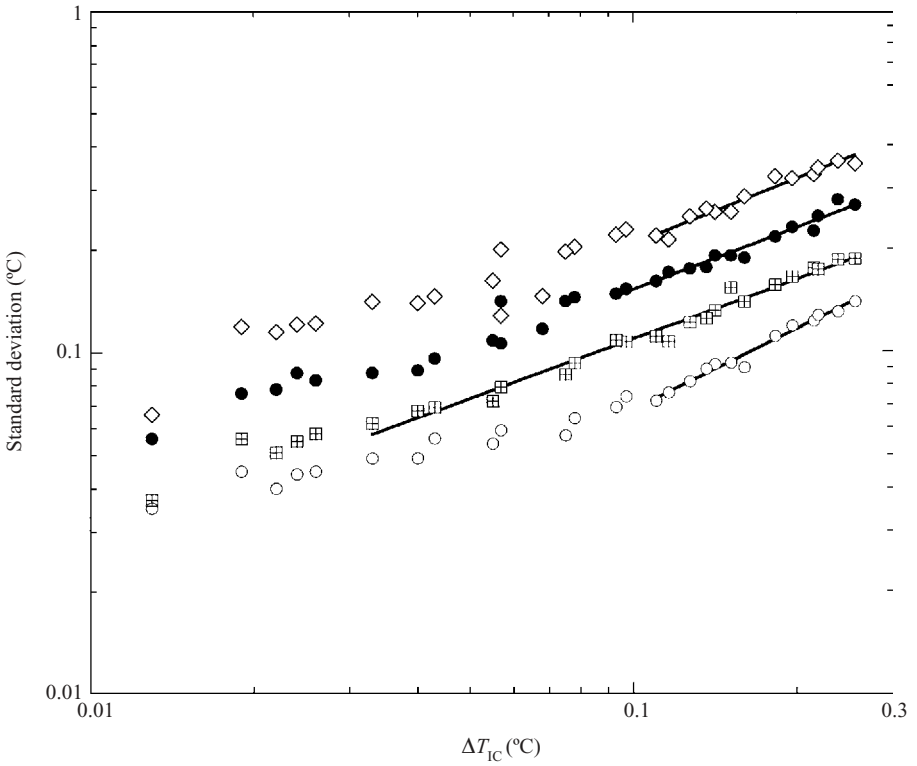

FIGURE 5. Standard deviation of temperature fluctuations versus the temperature rise of the circulating water through the inner sphere. Probes are located at four different distances from the inner boundary ($r = 1.5$, 3.1, 5.6, 8.1 cm), and are at the equatorial plane. The power-law fit for each probe is as follows: $T' = 0.89\Delta T_{IC}^{0.63}$ at $r = 1.5$ cm, $T' = 0.61\Delta T_{IC}^{0.60}$ at $r = 3.1$ cm, $T' = 0.41\Delta T_{IC}^{0.58}$ at $r = 5.6$ cm, $T' = 0.41\Delta T_{IC}^{0.78}$ at $r = 8.1$ cm.

them as intermittent bursts of cold plumes. The interpretation by Sumita & Olson (2002) involved the transport of columnar vortices in rotating convection. In rotating spherical convection, cyclonic vortices are larger than anticyclonic vortices, because of the Ekman boundary layer pumping, and the azimuthal transport of these unequal vortices produces asymmetric temperature fluctuations. The azimuthal transport of vortices is indicated by flow measurements described in the next section, and is in accord with measurements by Sumita & Olson (2002) in water at lower Rayleigh numbers.

The frequency power spectra for the records in figure 6 are shown in figure 8. These spectra are normalized so that the total power is unity. Each power spectrum is characterized by low-frequency and high-frequency parts with weak and strong frequency dependences, respectively. The silicone oil experiments at higher Rayleigh number have more power in the high-frequency range, which is evident from the time series records in figure 6. Fitting the high-frequency part to a power-law f^{-n} gives an exponent of $n = 1.72 \pm 0.06 (0.06 < f < 0.5\,\text{Hz})$ for $Ra/Ra_c = 634$ (silicone oil) and $n = 3.27 \pm 0.06 (0.08 < f < 0.5\,\text{Hz})$ for $Ra/Ra_c = 53$ (water).

3.1.3. *Flow structure*

The flow structures observed in these experiments correspond to the dual convective regime reported by Sumita & Olson (2000). In this regime, the convection is driven by

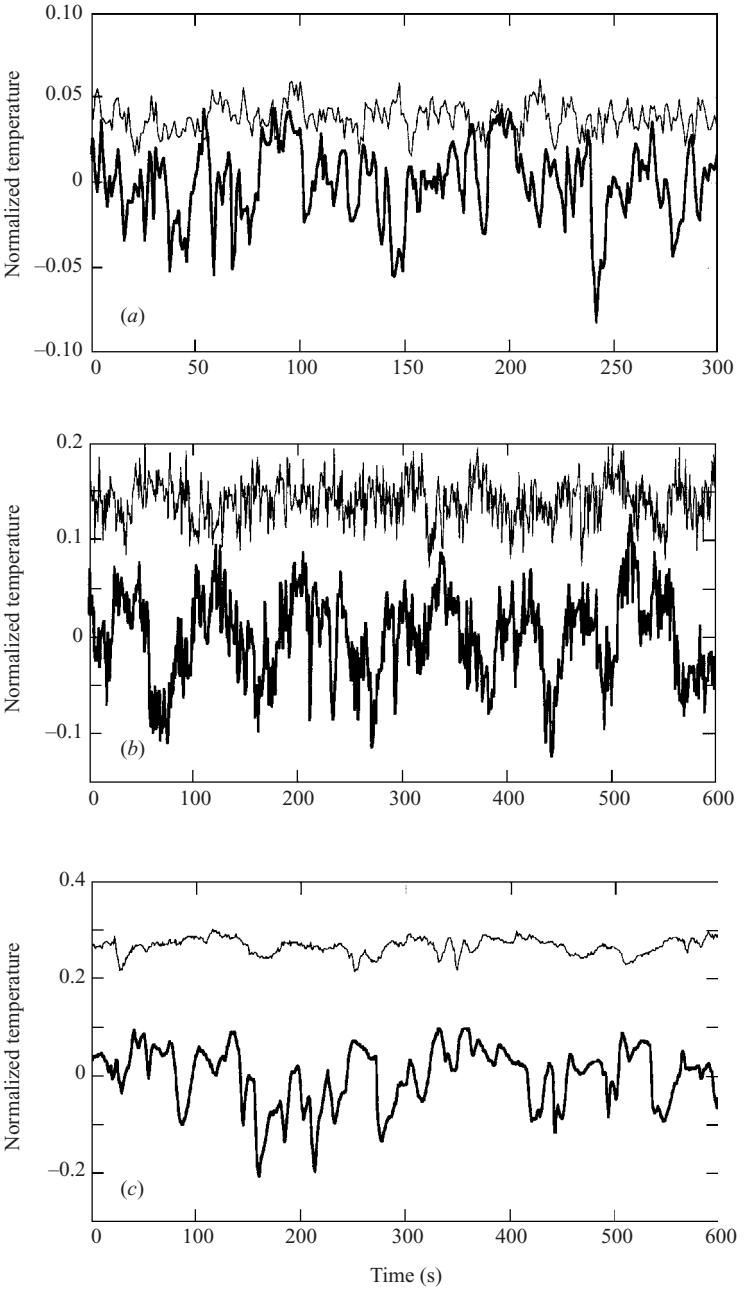

FIGURE 6. Examples of temperature time series from thermal convection in silicone oil in a rotating hemisphere: (*a*) $Ra/Ra_c = 634\,(\Delta T = 14.3\,^{\circ}\mathrm{C})$, (*b*) $Ra/Ra_c = 63\,(\Delta T = 0.20\,^{\circ}\mathrm{C})$; and water: (*c*) $Ra/Ra_c = 53\,(\Delta T = 13.85\,^{\circ}\mathrm{C})$. Temperature measurements at the innermost probe (1.5 cm from the inner boundary) are shown by thick lines, and those at the outermost probe (8.1 cm from the inner boundary) are shown by thin lines. Temperature T is normalized as $(T - \bar{T}_{1.5})/\Delta T$, where $\bar{T}_{1.5}$ is the average temperature of the innermost probe, and ΔT is the temperature difference across the shell.

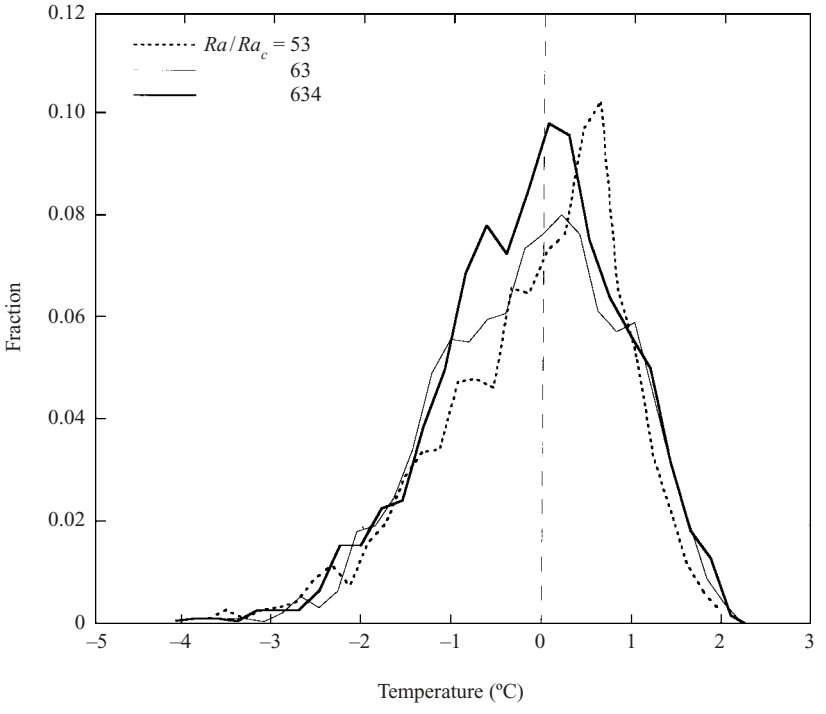

FIGURE 7. Histograms of temperature fluctuations around the mean for the temperature measurements at 1.5 cm from the inner boundary corresponding to the data shown in figure 6. Temperature is normalized by the standard deviation of temperature fluctuations.

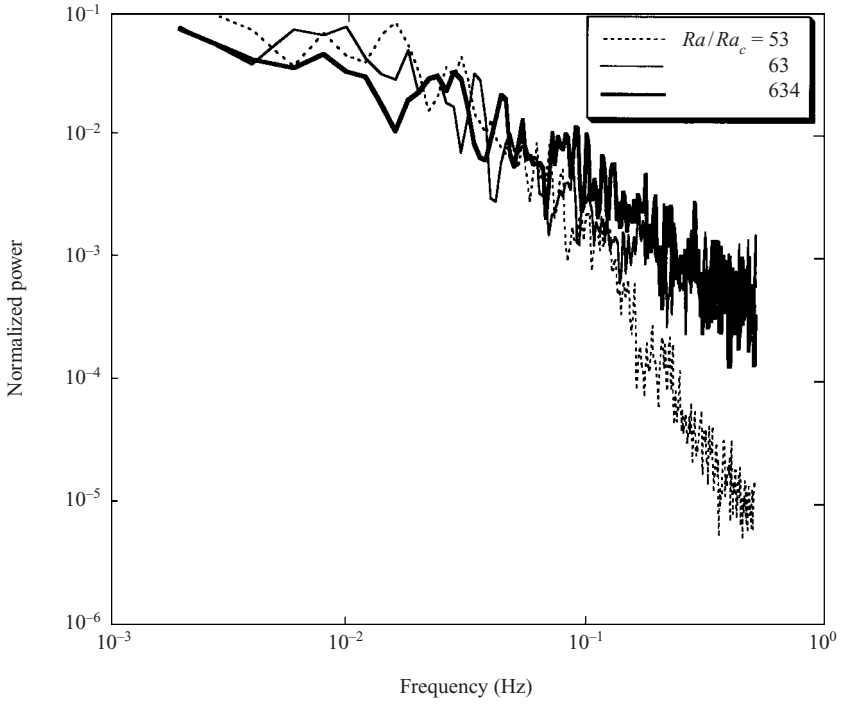

FIGURE 8. Power spectra of temperature fluctuations for the data source shown in figure 6.

serpentine nearly two-dimensional plumes originating from both the inner and outer boundaries, which form curtain-like cylindrical structures parallel to the rotating axis. Although we could not visually confirm this two-dimensionality of the flow in the present experiments, we can infer a geostrophic balance by estimating A, the ratio of buoyancy and Coriolis forces (Cardin & Olson 1994)

$$A = \frac{\alpha g T'}{\Omega V}. \tag{3.1}$$

Here, V is a characteristic convective velocity and T' is a characteristic temperature fluctuation associated with the convection. Substituting $T' = 0.13\,^{\circ}\mathrm{C}$ and $V = 3\,\mathrm{mm\,s^{-1}}$, typical values at mid-shell for $Ra/Ra_c \sim 250$, gives $A \simeq 0.03$, indicating that the force balance is quasi-geostrophic and that the flow should be nearly two-dimensional.

The average zonal velocity was measured by releasing neutrally buoyant fluid parcels into the convecting fluid. By tracking the parcels released at different radial distances from the inner boundary, we find that the zonal flow is westward at all Rayleigh numbers we have studied. For example, at $Ra/Ra_c = 254$ the westward flow is $V_\phi = 3\,\mathrm{mm\,s^{-1}}$ (Rossby number, $Ro = V/\Omega D = 1.4 \times 10^{-3}$) which is about an order of magnitude larger than that at $Ra/Ra_c = 44$ using water (Sumita & Olson 2000). We were not able to measure the radial flow velocity, but according to the results of weakly nonlinear theory (Zhang 1992), we can estimate that the radial flow should be faster than the zonal flow, a situation found at lower Prandtl number (Sumita & Olson 2000).

3.2. *Two-layered convection*

We have performed a series of experiments on layered convection, using two immiscible fluids to produce a stable density stratification. The temperature difference across the shell is fixed at $\Delta T = 11.15 \pm 0.52\,^{\circ}\mathrm{C}$ in these cases, and we vary the thickness ratio of the two layers. We use 1 cSt silicone oil for the inner layer and water for the outer layer. A similar set of two immiscible fluids was previously used by Hart (1972), but in a cylindrical geometry and at much lower rotation rates.

The interface between the layers assumes a parabolic shape, a result of the combined effect of centrifugal acceleration and laboratory gravity. We define the characteristic thickness of the inner and outer layers as the thickness of each layer in the equatorial plane. For the rotation rate used in this study (206 r.p.m.), the interface between the two layers intersects the outer boundary when the thickness of the inner layer is greater than 3 cm. The density contrast between these two layers is

$$\frac{\Delta\rho}{\rho} = 2\frac{(\rho_o - \rho_i)}{(\rho_o + \rho_i)} \simeq 0.203 \tag{3.2}$$

where subscripts i and o denote inner and outer layers respectively. The influence of the stratification can be estimated by comparing buoyancy frequency to rotation rate,

$$\frac{2\pi}{\Omega}\sqrt{\frac{\Delta\rho g}{\rho\delta}} \simeq 2\pi\sqrt{\frac{\Delta\rho}{\rho}\frac{D}{\delta}} \simeq 34. \tag{3.3}$$

Here δ is the typical size of the plume and we estimate it using a thermal boundary layer thickness of $\simeq 0.7$ mm obtained using the evaluation which follows. This estimate shows that the stratification effects dominate over instabilities related to rotation.

The convective pattern in the outer layer is basically the same as that for single-layered convection. It consists of plumes with a wavenumber of about 108 for all

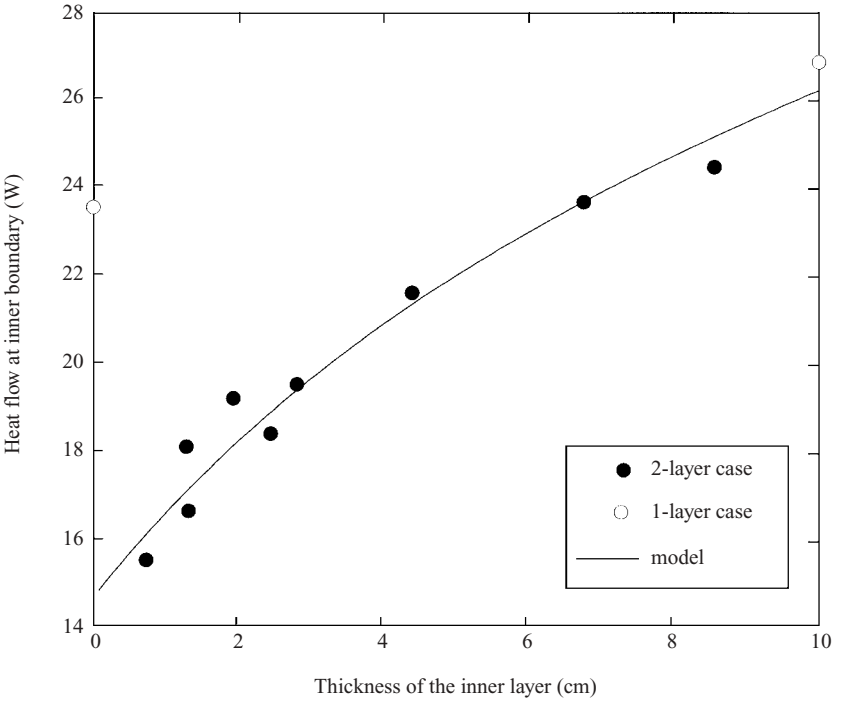

FIGURE 9. The relation between the thickness of the inner layer of silicone oil and the heat flow at the inner boundary in two-layer convection in a rotating hemispherical shell. The temperature difference across the inner and outer boundaries is $\Delta T = 11.15 \pm 0.52\,^{\circ}\mathrm{C}$. The best-fit scaling law for layered cases (shown as filled circles) is for $a = 12.75$ (see text). The data shown as open circles are the single-layered case.

thicknesses of the outer layer we examined. By tracking the motion of coloured tracers, we infer that the average zonal flow is westward, the same as found in the single-layer cases. Note that the fluid interface approximates a stress-free condition, so that each layer has one nearly free boundary and one rigid boundary. The insensitivity of the zonal flow direction to the exact mechanical boundary conditions may be a consequence of small Ekman number and hence very thin Ekman boundary layers (Zhang & Jones 1993). The flow velocity is, however, slower for layered convection, which is consistent with the lower heat flux and generally smaller kinetic energy compared to single-layer convection.

Statistics of temperature fluctuations for the layered convection cases indicate important differences with the single-layer cases. Where the outer layer is thin (thickness $< 5\,\mathrm{cm}$) the temperature fluctuations in the outer layer ($r = 8.1\,\mathrm{cm}$) show positive spikes (skewness). This suggests that the warm plumes dominate over cold plumes, which is in contrast to the single-layer case, where the skewness is always negative implying that the cold plumes dominate over warm plumes. We interpret this to be a consequence of the two layers, which inhibits cold plumes originating from the inner core penetrating into the outer layer.

In two-layered convection we find that heat flow and the radial temperature structure vary systematically with the thickness ratio. Figure 9 shows how the flow changes as the thickness of the inner layer increases. Heat flow decreases in a stepwise manner when there is a thin layer of silicone oil above the inner boundary, and then

gradually increases with the thickness of the inner layer. The radial temperature profile also changes in a corresponding way, and the thermal boundary layer adjacent to the inner boundary becomes thinner as the thickness of the inner layer increases.

The following is a qualitative explanation for the thickness dependence of heat flow in layered convection. Because of the spherical geometry, the conductive radial temperature profile has its steepest gradient at the inner boundary. In the presence of convection, this gradient is further steepened, so that most of the temperature change in the fluid is localized there. This localization of the thermal gradient also occurs in a layered spherical shell, unless the outer layer is a thermal insulator and is not convecting. In our experiments, the outer water layer is in fact more conductive (by about a factor of 6) than the inner silicone oil layer, so the first situation applies. As a result, with increasing thickness of the inner layer, the temperature at the fluid interface asymptotically approaches the temperature of the outer boundary. We emphasize that this tendency is enhanced by convection. The conductive temperature profile of a layered system where the thermal conductivity of the inner layer is smaller than the outer layer ($k_i < k_o$) in either spherical or cylindrical geometry gives rise to smaller heat flux at the inner boundary as the thickness of the inner layer increases, and is opposite to what we observe in our experiments.

A quantitative estimate of the dependence of heat flow on layer thickness can be constructed using the following arguments. First we assume the radial temperature profile is similar to the one shown schematically in figure 10. For simplicity we have neglected the thermal boundary layer in the outer region of each layer, because the temperature drop there is small compared to that in the inner boundary region of each layer, another consequence of the spherical geometry. Heat flow at the inner surface of each layer can be written as

$$q_i = k_i \frac{\Delta T_i}{\delta_i}, \tag{3.4}$$

$$q_o = k_o \frac{\Delta T_o}{\delta_o}. \tag{3.5}$$

The thickness of the thermal boundary layer can be calculated as follows. We assume the heat transfer law $Nu \propto Ra^{1/3}$, which approximately agrees with our measurements. According to this law, the thickness of the thermal boundary layer is independent of the total thickness of the layer. In addition, the measurements by Rossby (1969) showed that the Nusselt number of rotating convection is approximately independent of the Ekman number for $Ra/Ra_c > 10$. Our experiments meet this condition. A quantitative verification of this can be made by comparing the Nusselt number for non-rotating Rayleigh–Bénard experiments using water with our Nusselt number at the same Rayleigh numbers. Using $Nu = 0.19Ra^{0.28}$ (Qiu & Xia 1998), we obtain $Nu = 67$–127 for a Rayleigh number range of $Ra = 1.24 \times 10^9$–1.24×10^{10}. This is similar to our measurements of $Nu = 40$–186 for $Ra = 1.24 \times 10^9$–1.24×10^{10}. Together, these imply that the thickness of the thermal boundary layer varies as

$$\delta_i = a D_i Ra_i^{-1/3}, \tag{3.6}$$

$$\delta_o = a D_o Ra_o^{-1/3}, \tag{3.7}$$

where D is the layer thickness, and a is a constant coefficient. This form for the thermal boundary layer thickness in a rotating thermal convection has been previously used by Sakai (1997). Finally, the total heat flow at the inner surface of the inner and outer

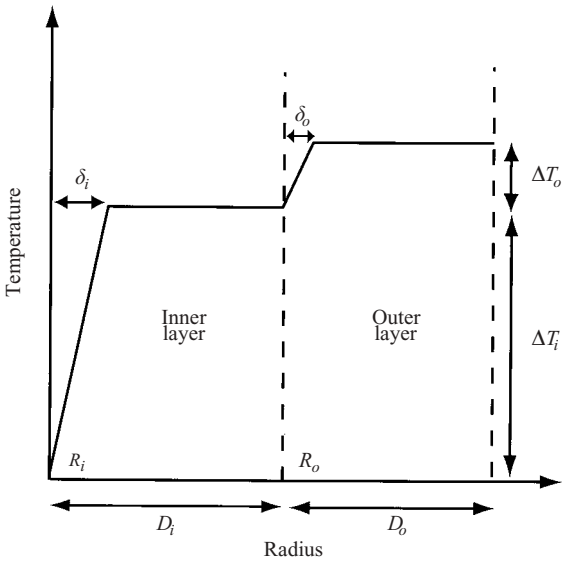

FIGURE 10. A schematic diagram showing the radial temperature profile which is used to model the thickness dependence of heat flow shown in figure 9.

surfaces must balance, so that

$$R_i^2 q_i = R_o^2 q_o, \tag{3.8}$$

where R_i and $R_o = R_i + D_i$ are the radii at the inner surface of each layer. Using the above relations we find $\Delta T_o / \Delta T_i$ as

$$\frac{\Delta T_o}{\Delta T_i} = \left(\frac{\alpha_i g_i \kappa_o \nu_o}{\alpha_o g_o \kappa_i \nu_i} \right)^{1/4} \left(\frac{k_i}{k_o} \right)^{3/4} \left(\frac{R_i}{R_o} \right)^{3/2}. \tag{3.9}$$

In the simpler case where the material properties in the two layers are identical, (3.9) reduces to

$$\frac{\Delta T_o}{\Delta T_i} = \left(\frac{g_i}{g_o} \right)^{1/4} \left(\frac{R_i}{R_o} \right)^{3/2}, \tag{3.10}$$

which is a decreasing function of D_i, indicating that the interfacial temperature approaches the temperature of the outer boundary as D_i increases. From (3.4) and (3.6), we obtain $q_i \propto \Delta T_i^{4/3} g_i^{1/3}$ showing that the heat flow at the inner boundary would increase with D_i, consistent with the measurements. We note that similar experiments and analyses for non-rotating layered thermal convection in a cylindrical geometry were performed by Namiki & Kurita (2003).

In figure 9, we fit the temperature data by the least-squares method and obtain the prefactor $a = 12.75$. Using this value, we can calculate the average thickness of the thermal boundary layer as $\delta \simeq 0.7$ mm. We also tried to fit the data using the heat transfer relation $Nu \propto Ra^{2/7}$, but this gave a poorer fit.

4. Implications for convection in the Earth's core

The temperature profile in the Earth's core probably resembles the temperature profile in our experiments in several important respects. In particular, because the Earth's inner core is an important energy source, it is probable there is a thermal boundary layer near the inner core boundary (ICB). Furthermore, convection has

probably mixed the fluid outer core so the temperature profile there closely follows an adiabat. It is also probable there is a thermal boundary layer below the core–mantle boundary (CMB), although it is unlikely to be as strong as that above the ICB, for the following reasons.

A typical estimate of the heat flux at the CMB is $q_{\mathrm{CMB}} \simeq 20\,\mathrm{mW\,m^{-2}}$, which is comparable to the heat flux conducted down the core adiabat, $q_{\mathrm{ad}}^{\mathrm{CMB}} \simeq 18\,\mathrm{mW\,m^{-2}}$ (see Sumita & Yoshida 2002, for a review):

$$q_{\mathrm{CMB}} \sim q_{\mathrm{ad}}^{\mathrm{CMB}}. \tag{4.1}$$

This implies that the temperature gradient in the thermal boundary layer beneath the CMB is close to the adiabat. On the other hand, as a consequence of the smaller radial pressure gradient, the adiabatic temperature gradient near the ICB is less steep than that near the CMB. The heat conducted down the adiabatic thermal gradients at the two boundaries are related approximately as

$$q_{\mathrm{ad}}^{\mathrm{ICB}} \sim 0.4 q_{\mathrm{ad}}^{\mathrm{CMB}}. \tag{4.2}$$

Considerations of the heat budget for the core indicate that about 1/3 of the heat loss from the core is from the inner core, so that $Q_{\mathrm{ICB}}/Q_{\mathrm{CMB}} \sim 1/3$. From this it follows that

$$\frac{q_{ICB}}{q_{CMB}} = \frac{Q_{\mathrm{ICB}}}{Q_{\mathrm{CMB}}} \frac{4\pi R_{CMB}^2}{4\pi R_{ICB}^2} \sim 3. \tag{4.3}$$

From the above relations, we obtain

$$\frac{q_{\mathrm{ad}}^{ICB}}{q_{ICB}} \sim 0.1 \frac{q_{\mathrm{ad}}^{CMB}}{q_{CMB}} \sim 0.1. \tag{4.4}$$

This result indicates that the temperature gradient in the thermal boundary layer immediately above the ICB is approximately 10 times steeper than the adiabat. Therefore the basic temperature structure in our experiments is similar to the basic temperature structure in the core with the adiabatic gradient removed.

There are two simple models of possible stable stratification in the Earth's outer core that are consistent with the formation of the inner core: a light (low-density) layer at the top of the core, or alternatively, a heavy (high-density) layer just above the inner core. In either case we may reasonably assume that the thermal conductivities of the two layers are comparable, since both layers are iron-rich liquids. Our experiments indicate that the heat flow at the inner core boundary would be strongly suppressed by a thin dense layer at the bottom of the core, and not as strongly affected by a light layer at the top of the core. A dense layer at the bottom of the outer core could be an iron-rich liquid depleted in lighter elements. Such a layer could suppress heat transfer and inner core solidification, and might even result in melting of the inner core. Alternatively, it may form from settling of solid iron particles, forming a slurry. There are several lines of seismological evidence suggesting that a stably stratified layer exists above the ICB (Souriau & Poupinet 1991; Song & Helmberger 1995). In addition, other lines of seismological evidence indicate a possible stably stratified layer beneath the CMB (Lay & Young 1990). Our experiments indicate that this layer would have a smaller effect on heat transfer than a stably stratified layer above the inner core.

5. Summary

We have conducted thermal convection experiments in a rapidly rotating hemispherical shell at Ekman number $Ek = 4.7 \times 10^{-6}$ and Rayleigh numbers up to $Ra \simeq 612 Ra_c$. We find that the temperature gradient in the fluid becomes nearly isothermal as a consequence of vigorous convection, with a thin thermal boundary layer above the inner boundary. Convective heat measurements indicate a power-law relationship between the Nusselt number and the Rayleigh number with an exponent of about 0.4. The amplitude of temperature fluctuations is in accord with the simple geostrophic turbulence model of Cardin & Olson (1994). Experiments on layered convection in the same spherical shell geometry show that heat transfer is less than in single-layer convection, and in particular, heat transfer is strongly inhibited by a thin layer above the inner boundary.

We thank J. Aubert for sending a preprint prior to publication. I.S. was supported by the Japan Society for the Promotion of Science postdoctoral fellowships for research abroad during which the experiments were carried out at Johns Hopkins University. The experiments were supported by the Geophysics Program of NSF and NASA grant NAG5-11220.

REFERENCES

Aubert, J., Brito, D., Nataf, H.-C., Cardin, P. & Masson, J.-P. 2001 A systematic study of rapidly rotating spherical shell convection in water and liquid gallium. *Phys. Earth Planet. Inter.* **128**, 51–74.

Belmonte, A. & Libchaber, A. 1996 Thermal signature of plumes in turbulent convection: The skewness of the derivative. *Phys. Rev.* E **53**, 4893–4898.

Boubnov, B. M. & Golitsyn, G. S. 1986 Experimental study of convective structures in rotating fluids. *J. Fluid Mech.* **167**, 503–531.

Boubnov, B. M. & Golitsyn, G. S. 1990 Temperature and velocity field regimes of convective motions in a rotating plane fluid layer. *J. Fluid Mech.* **219**, 215–239.

Busse, F. H. 1970 Thermal instabilities in rapidly rotating systems. *J. Fluid Mech.* **44**, 441–460.

Busse, F. H. & Carrigan, C. R. 1974 Convection induced by centrifugal buoyancy. *J Fluid Mech.* **62**, 579–592.

Busse, F. H. & Carrigan, C. R. 1976 Laboratory simulation of thermal convection in rotating planets and stars. *Science* **191**, 81–83.

Cardin, P. & Olson, P. 1994 Chaotic thermal convection in a rapidly rotating spherical shell: consequences for flow in the outer core. *Phys. Earth Planet Inter.* **82**, 235–259.

Hart, J. E. 1972 A laboratory study of baroclinic instability. *Geophys. Fluid Dyn.* **3**, 181–209.

Jones, C. A., Soward, A. M. & Mussa, A. I. 2000 The onset of thermal convection in a rapidly rotating sphere. *J. Fluid Mech.* **405**, 157–170.

Lay, T. & Young, C. J. 1990 The stably-stratified outermost core revisited. *Geophys. Res. Lett.* **17**, 2001–2004.

Manneville, J.-B. & Olson, P. 1996 Banded convection in rotating fluid spheres and the circulation of the Jovian atmosphere. *Icarus* **122**, 242–250.

Namiki, A. & Kurita, K. 2003 Heat transfer and interfacial temperature of two-layered convection: Implications for the D″-mantle coupling, *Geophys. Res. Lett.* **30**, 10.1029/2002GL015809.

Qiu, X.-L. & Xia, K.-Q. 1998 Viscous boundary layers at the sidewall of a convection cell. *Phys. Rev.* E **58**, 486–491.

Rossby, H. T. 1969 A study of Bénard convection with and without rotation. *J. Fluid Mech.* **36**, 309–335.

Sakai, S. 1997 The horizontal scale of rotating convection in the geostrophic regime. *J. Fluid Mech.* **333**, 85–95.

Song, X. & Helmberger, D. V. 1995 A P wave velocity model of the Earth's core. *J. Geophys. Res.* **100**, 9817–9830.

Souriau, A. & Poupinet, G. 1991 The velocity profile at the base of the liquid core from PKP(BC+Cdiff) data: an argument in favour of radial inhomogeneity. *Geophys. Res. Lett.* **18**, 2023–2026.

Sumita, I. & Olson, P. 2000 Laboratory experiments on high Rayleigh number thermal convection in a rapidly rotating hemispherical shell. *Phys. Earth Planet Inter.* **117**, 153–170.

Sumita, I. & Olson, P. 2002 Rotating thermal convection experiments in a hemispherical shell with heterogeneous boundary heat flux: Implications for the Earth's core. *J. Geophys. Res.* **107**, 10.1029/2001JB000548.

Sumita, I. & Yoshida, S. 2002 Thermal interactions between the mantle, outer and inner cores, and the resulting structural evolution of the core. In *Earth's Core: Dynamics, Structure, Rotation* (ed. Dehant, V. *et al.*) Geodynamics Series, vol. 31, pp. 213–231. American Geophysical Union.

Zhang, K. 1992 Spiralling columnar convection in a rapidly rotating spherical fluid shells. *J. Fluid Mech.* **236**, 535–556.

Zhang, K. & Jones, C. A. 1993 The influence of Ekman boundary layers on rotating convection. *Geophys. Astrophys. Fluid Dyn.* **71**, 145–163.

Zhang, K. & Schubert, G. 2000 Magnetohydrodynamics in spherical systems. *Annu. Rev. Fluid Mech.* **32**, 409–443.